A Battery Degradation Model for Cost-Optimized PV-BESS Design in Telecom Base Stations

A Battery Degradation Model for Cost-Optimized PV-BESS Design in Telecom Base Stations

Mohammad Reza Jokar, Michela Meo, Greta Vallero, Daniela Renga
Politecnico di Torino, Italy,
Email: mohammadreza.jokar@polito.it

***Abstract*—Telecom base stations increasingly rely on solar power and battery storage to achieve sustainable, cost-effective energy solutions, but battery degradation poses a significant challenge to system reliability and longevity. This paper introduces an innovative optimization framework that accounts for lithium-ion battery aging, modeling both calendar and cycle degradation with a novel segment-based approach. Designed for seamless integration into cost-effective energy planning, the framework optimizes photovoltaic (PV) panel and battery sizing to minimize costs and extend system lifespan. Validated using real-world base station power consumption data, our approach outperforms traditional rainflow-based aging models, reducing battery cycle wear by up to 65.5% compared to aging-unaware methods and by an additional 10% over rainflow-based methods. By enabling real-time battery health tracking, it supports dynamic energy management, offering a practical solution for sustainable telecom networks.**

***Index Terms*—Battery aging, photovoltaic sizing, energy optimization, base stations, sustainable telecom networks, segment-based modeling**

I. Introduction

To cope with the ever-increasing energy demand of the mobile access network, which is expected to increase by 289% between 2020 and 2035, as highlighted in [1], a promising approach is incorporating local renewable energy source (RES) harvesting systems, which power the base stations (BSs) through sources such as solar photovoltaic (PV) and wind, along with energy storage and the power grid [2], [3]. While the efficacy of this approach has been largely demonstrated in the literature, optimistic assumptions that neglect the degradation during the design and operation of battery energy storage systems (BESSs) are often made, which may lead to misleading costs and suboptimal system design [4].

Battery degradation significantly impacts the lifetime and economic viability of energy storage. Batteries experience two common degradation mechanisms: (i) calendar aging, i.e., time aging [5], and (ii) cycle aging, i.e., charge/discharge cycle-induced aging [6]. These two mechanisms reduce the effective usable capacity of the battery. The assumption of constant capacity is a naive simplification ignoring the dynamic interplay between demand, renewable output, operating conditions, and the effects of degradation. Dominant operational conditions that influence aging include Depth of Discharge (DoD), State of Charge (SOC), and temperature. Higher DoD accelerates cycle aging and diminishes battery life, necessitating an on-use duration compromise [5]. The non-linear relationship between DoD and battery life has been investigated, and the financial impact estimation models of DoD highlight the importance of incorporating degradation costs into system design [5].

Current battery degradation models are informative but rely on simplifying assumptions, without considering the impact of significant parameters like DoD, SOC, and ambient conditions, as in [8]. In response to these limitations, more sophisticated models were introduced. Although more advanced techniques such as Rainflow counting are more accurate because they detect cycle depths, they are not applicable in real time or implementable within optimization routines such as Mixed-Integer Linear Programming (MILP) for battery use optimization [9]. Rainflow needs full cycle completion and offline calculation, thus resulting in less suitable for step-by-step decision-making that is needed in system sizing and energy management. Such research gaps underline the need for accurate, real-time, and computationally tractable battery degradation models that could be used within planning and operational frameworks.

For this purpose, we present a segment-based degradation model that calculates aging via DoD transitions in every time interval so that it can be easily incorporated into planning and operational frameworks. We are dealing with a BS which is equipped with a PV panel, a battery, and is also connected to the electric grid. We calculate the optimal capacity of the PV panel and battery for achieving cost minimisation, considering battery degradation. Specifically, the contributions of our study are summarised as follows:

- present a segment-based battery aging model that tracks depth-of-discharge shifts at each time step for accurate degradation modelling. Unlike the Rainflow method, which is offline and computationally intensive, our approach supports real-time MILP optimization, enabling efficient energy management in dynamic systems.
- formulate a MILP optimization framework that incorporates both cycle and calendar aging in PV-battery system design. The model jointly optimizes PV and battery capacities to minimize capital and operational expenses.

II. System planning and BESS Degradation Model

In this paper, we consider the structure illustrated in Fig. 1. The system consists of a multi-frequency BS, powered by a PV panel, battery, and power grid. The system also includes a DC bus for power distribution. The PV panel provides DC

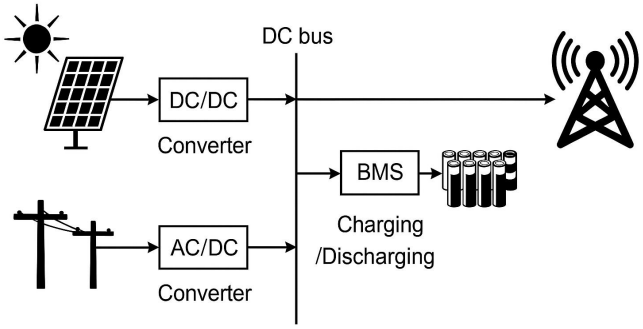

Fig. 1: System architecture of the proposed hybrid energy management system.

power through a DC/DC converter and the grid through an AC/DC converter. To integrate BESS capacity degradation into energy management, it is essential to model the degradation process and estimate its impact on battery lifespan. Degradation occurs due to calendar aging, which refers to the degradation over time, and cycle aging, which is the degradation from charge/discharge cycles. Both aging mechanisms reduce battery health and usable capacity over time, highlighting the need for a comprehensive approach to accurately estimate the rate of capacity degradation and incorporate associated costs into an optimised BS supply system.

A. Calendar Aging

Calendar aging is the gradual loss of battery capacity even when not cycled. Temperature, SOC, and time affect this aging process. In [5], the cumulative calendar aging (expressed as a percentage of the initial installed capacity faded up to hour h, that is denoted as AG_{cal}^{Ch}, is formalised with the following non-linear model:

$$AG_{\text{cal}}^{Ch} = (k_t \cdot h)^{b_t} \cdot \left[k_{\text{soc}} \cdot \text{SOC}_h^{b_s} + k_c\right] \cdot e^{k_T \cdot (T_h - T_{\text{ref}})} \quad (1)$$

where SOC_h is the SOC (%) at time h, T_h is the operating temperature at the same time, and T_{ref} is the reference temperature, 25 °C in [5]. The parameters k_t, k_{soc}, k_c, and k_T are empirically calibrated using experimental battery data in [5], and also the exponents b_t and b_s, that represent the non-linearity of time and SOC dependencies.

The non-linear calendar aging model is computationally intensive for optimization frameworks. To mitigate this, the model is linearized through regression, preserving its predictive accuracy. This linearization yields the following outcome:

$$AG_{\text{cal}}^{Ch} = (k_t \cdot h)^{0.8} \cdot (a_1 \cdot \text{SOC}_h + a_2 \cdot T_h) \quad (2)$$

where a_1, and a_2 are coefficients derived from regression analysis. To further simplify calculations, the linearized model is expressed in a discretized form for incremental time steps as follows:

$$AG_{\text{cal}}^{h} = \left[(k_t \cdot h)^{0.8} - (k_t \cdot (h-1))^{0.8}\right] \cdot (a_1 \cdot \text{SOC}_h + a_2 \cdot T_h) \quad (3)$$

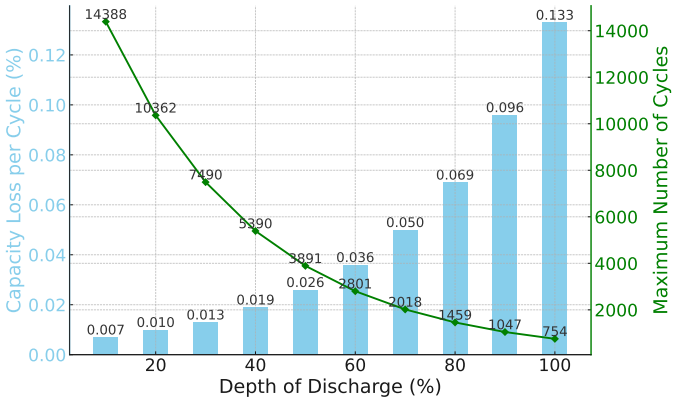

Fig. 2: Relationship between DoD and battery cycle degradation at $T = 25°C$ see Eq. 4 and data in [6].

This discretized formulation allows efficient calculation of hourly calendar aging (%), directly based on the battery state in a linear form.

B. Cycle Aging

Cycle aging is the progressive loss of battery capacity due to repeated charge and discharge, and is heavily dependent on operating conditions such as DoD, temperature, and energy throughput [7]. A popular model for approximating the number of cycles a battery can tolerate at a specified DoD is given in [5], as follows:

$$N_{\text{T}}^{\text{DoD}} = \left(\frac{C_{\text{s}} \cdot \text{DoD}_n^{p_{\text{DoD}}} \cdot \exp(k_D \cdot (T_h))}{1 - \text{RT}}\right)^2 \quad (4)$$

Here, $N_{\text{T}}^{\text{DoD}}$ represents the number of complete cycles the battery can undergo at a specific DoD and temperature T before reaching end-of-life. RT denotes a fractional threshold at which the battery is replaced, typically set to 0.8 as described in [5]. This threshold triggers the replacement process when the battery capacity falls below this fraction of the nominal capacity. C_{s} is an empirical scaling factor; p_{DoD} captures the nonlinear dependence on DoD; and k_D reflects the temperature sensitivity of aging. Eq. (4) links the aging effect per cycle to DoD and temperature.

Assuming a constant temperature of 25°C (as result of cooling system), the relationship defined by (4) yields a non-linear dependency between DoD and cycle life, as shown in Fig. 2. The green line in the graph shows that as DoD increases, the number of achievable cycles decreases significantly, highlighting the impact of deep discharges on battery longevity. Importantly, Fig. 2 represents the cycle life of a battery under idealised, complete cycling conditions, where each cycle begins and ends at the full state of charge. However, in practical applications, batteries rarely operate under such ideal conditions. Instead, they experience a mix of *complete (CC)*, *incomplete (IC)*, and *partial cycles (PC)* due to dynamic operating conditions, variable loads, and stochastic user behaviour. The real-world cycling pattern necessitates a method capable of accurately estimating degradation across all cycle types in real time.

TABLE I: Model Parameters and Their Values

Variable	Value	Variable	Value	Variable	Value
T_h	25 (°C)	k_D	0.05	k_t	0.0014
a_1	0.0028	a_2	0.0019	p_{DoD}	0.4904
r	2.4%	C_{scale}	7.1568	k_T	0.02717
RT	80%	λ_{CR}	0.4	λ_{DR}	0.4
η_{Charge}	90%	$\eta_{\text{Discharge}}$	90%	$\kappa(E)$	\$0.20/kWh
N	20 years	$C_{\text{PV}}^{\text{Unit}}$	\$800/kW	$C_{\text{BESS}}^{\text{Unit}}$	\$300/kWh

To overcome the limitations of conventional cycle-counting models, we propose a novel, segment-based aging model that enables real-time calculation of degradation across arbitrary cycling patterns. The key idea is to track aging as a capacity loss curve with respect to the DoD. This concept is supported by experimental data, such as in Fig. 2, which illustrates the nonlinear relationship between DoD and capacity loss per full cycle. For simplicity, we consider that DoD can change in 10 steps from 0.1 to 1. The blue bars show that when DoD increases, capacity loss per cycle increases sharply—e.g., a full cycle at 100% DoD results in 0.133% loss, while at 20% DoD, the loss is only 0.010%.

Proposed Aging Formula: We define an aging function $AG_{Cycle}^{\text{segment}}$, where each DoD level corresponds to a known cycle capacity loss obtained from empirical data. Then, the aging that occurs in time step h, when the battery transitions from DoD_{h-1} to DoD_h, is computed as:

$$AG_{Cycle}^{\text{segment}} = AG_{DoD}^{\text{h}} - AG_{DoD}^{\text{h-1}} \tag{5}$$

This approach enables real-time aging estimation without requiring full cycle completion. It unifies the treatment of CC, IC, and PC and is well suited for integration into MILP optimization frameworks. For example, if the DoD increases from 60% to 90%, the aging, according to Fig. 2, is:

$$AG_{60\%to90\%}^{segment} = AG_{90\%} - AG_{60\%} = 0.096 - 0.036 = 0.060\%$$

More generally, the total aging over any period can be computed as:

$$AG_{cycle}^{Total} = \sum_{h=1}^{T} \left(AG_{DoD}^{h} - AG_{DoD}^{h-1} \right) \tag{6}$$

This formulation is consistent with cumulative capacity loss models and allows degradation to be tracked continuously using only the DoD trajectory.

To account for charge/discharge directionality and considering charging degradation, we refine the segment-level formula as:

$$AG_{Cycle}^{\text{segment}} = \frac{\left(AG_{\text{DoD}}^{\text{end}} - AG_{\text{DoD}}^{\text{start}} \right) \cdot \left[I_{\text{disch}}^{h} - I_{\text{ch}}^{h} \right]}{2} \tag{7}$$

Here, I_{disch}^{h} and I_{ch}^{h} are binary indicators for the battery operating state in hour h, and the division by 2 reflects the consideration of the degradation of charging. For mathematical details of the validation, see [5].

III. Problem Formulation Framework

We formulate the optimization problem to determine the capacity of the PV panel and battery that will yield the minimum CAPEX and OPEX costs. The problem is formulated as a MILP model, whose objective function consists of 1) investment costs, 2) grid energy costs, 3) battery degradation, 4) salvage value, and 5) penalties for curtailed renewable energy. This approach provides a balanced evaluation of economic and operational performance. The inputs include the hourly PV power generation, BS load consumption, and the temperature. Optimization variables include the size of the BESS, of the PV capacity, and the DoD throughout the time horizon, while other parameters are listed in Table I.

1) Objective Function: The objective comprehensively includes all operational and investment costs in monetary terms, ensuring an economically optimized system design:

$$C_{\text{T}} = \min \left(\sum_{h=1}^{N \cdot 8760} \frac{C_{\text{g}}^{h} + C_{\text{AG}}^{h} + C_{\text{PV-W}}^{h}}{(1+r)^{\lceil h/8760 \rceil - 1}} + C_{\text{inv}} - \frac{S_{\text{BESS}}}{(1+r)^{N}} \right) \tag{8}$$

where r is the annual inflation rate, N is the system lifetime (e.g., 25 years). C_{g}^{h}, C_{AG}^{h}, and $C_{\text{PV-W}}^{h}$ represent the grid energy costs, battery degradation costs, and penalties for curtailing PV energy at time h, respectively. In addition, C_{inv} is the total investment cost for PV panels and batteries. S_{BESS} is the salvage value of the battery at the end of its lifecycle and 8760 represents the total number of hours in a year.

Grid Cost: The cost of energy purchased from the grid at time h is defined as:

$$C_{\text{g}}^{h} = E_{\text{g}}^{h} \cdot \pi_{\text{g}}^{h} \tag{9}$$

where E_{g}^{h} is the energy purchased from the grid at time h and π_{g}^{h} is the inflation-adjusted price of grid electricity at time h.

Battery Degradation Cost: The degradation cost, C_{AG}^{h}, is the sum of the s of degradation due to calendar aging and cycle aging, computed as described in Section II:

$$C_{\text{AG}}^{h} = C_{Cal}^{h} + C_{Cycle}^{h} \tag{10}$$

$$C_{Cal}^{h} = DC_{\text{BESS}} \cdot AG_{\text{cal}}^{h} \tag{11}$$

$$C_{Cycle}^{h} = DC_{\text{BESS}} \cdot AG_{\text{Cycle}}^{h} \tag{12}$$

The degradation cost in Eq. (10) comprises two primary components: the calendar aging cost (C_{Cal}^{h}) and the cycle aging cost (C_{Cycle}^{h}). The AG_{cal}^{h} is determined using Eq. (3), and AG_{cycle}^{h} is derived from Eq. (7). In both Eq. (11) and (12), the parameter DC_{BESS} denotes the expense linked to battery deterioration per unit. The calculation is based on the battery's initial cost, incorporating any relevant discounts or credits, and is allocated over the battery's anticipated lifespan [10].Moreover, we implement a penalty for any amount of energy generated by the PV panel that is wasted, as it cannot be used immediately to power the BS nor stored in the battery

due to either full capacity or charging rate limitations. The cost of curtailment is expressed as:

$$C^h_{\text{PV-W}} = \kappa(E) \cdot E^h_{\text{W}} \tag{13}$$

where E^h_{W} is a non-negative variable representing the curtailed (i.e., wasted) energy, and $\kappa(E)$ is a penalty factor. Eq. 13 is subject to the following constraint:

$$E^h_{\text{W}} \geq E^h_{\text{PV}} - E^h_{\text{Load}} - E^h_{\text{Charge}} \tag{14}$$

Investment Cost: The investment cost includes PV panel and battery installation and purchase costs:

$$C_{\text{inv}} = (C^{\text{Unit}}_{\text{PV}} \cdot N_{\text{PV}}) + (C^{\text{Unit}}_{\text{BESS}} \cdot N_B) + C_{\text{install}} \tag{15}$$

where $C^{\text{Unit}}_{\text{PV}}$ and $C^{\text{Unit}}_{\text{BESS}}$ are the costs per unit capacity for PV and batteries, N_{PV} is the number of PV units (kW), N_{B} is the installed number of battery units (kWh), and C_{install} is the capital expenditure associated to the installation of batteries and PV. Battery replacements during the time horizon are added to the investment cost and adjusted to present value using the inflation rate. PV salvage value is neglected due to their 25-year lifetime, while battery salvage value is included in the objective based on remaining useful capacity that can be defined as S_{BESS}, which is calculated as:

$$S_{\text{BESS}} = \left(1 - \sum_{h=1}^{N \cdot 8760} AG^h_{\text{cycle}} + AG^h_{\text{cal}}\right) \cdot (C^{\text{Unit}}_{\text{BESS}} \cdot BESS_{\text{I}}) \tag{16}$$

The initial installed capacity of the battery, which is denoted $BESS_I$, decreases over the time horizon due to degradation caused by AG^h_{Cal} and AG^h_{Cycle}. Let us denote as $BESS^h_{\text{d\_b\_r}}$ the available capacity of the battery at time h before a replacement is needed. The value of $BESS^h_{\text{d\_b\_r}}$ is updated by subtracting the combined degradation effects from the previous capacity at each time step, as follows:

$$BESS^h_{\text{d\_b\_r}} = BESS^{h-1}_{\text{D}} - (AG^h_{\text{Cal}} + AG^h_{\text{Cycle}}) \cdot BESS_{\text{I}} \tag{17}$$

where $BESS^{h-1}_{\text{D}}$ represents the available capacity of the BESS at time $(h-1)$. A replacement mechanism is triggered if the BESS is fully degraded. For this constraint we use the big M method, which is completely described in [11]. The binary variable $R^h_{\text{b\_t}}$ resets the capacity to its initial value when replacement occurs, and it is 1 if $BESS^h_{\text{D}} \geq BESS_{\text{I}}$, 0 otherwise. This means that the available capacity of the BESS at time h is derived as follows:

$$BESS^h_{\text{D}} = R^h_{\text{b\_t}} \cdot BESS_{\text{I}} + (1 - R^h_{\text{b\_t}}) \cdot BESS^h_{\text{d\_b\_r}} \tag{18}$$

$$BESS^h_{\text{D}} \geq RT \cdot BESS_{\text{I}} - M \cdot (1 - R^h_{\text{b\_t}}) \tag{19}$$

$$BESS^h_{\text{D}} \leq R^h_{\text{b\_t}} \cdot M + RT \cdot BESS_{\text{I}} \tag{20}$$

$$R^h_{\text{b\_t}} \in \{0, 1\} \tag{21}$$

PV Panel Generation Constraints: The power generated by PV panels at any time h is constrained by operational limits expressed as $0 \leq P_{\text{PV}}(h) \leq P_{\text{PV, max}}(h)$.

BESS Constraints: At any time h, the BESS is limited by its charging and discharging power, energy balance, SOC, DoD, and degradation tracking. The BESS absorbs or delivers power at time h, denoted as P^h_{Ch} and P^h_{Disch}, respectively. These powers are limited by maximum charging λ_{CR} and discharging λ_{DR} rates, which are fractions of the $BESS^h_{\text{D}}$, as follows:

$$P^h_{\text{Ch}} \leq \lambda_{\text{CR}} \cdot BESS^h_{\text{D}} \tag{22}$$

$$P^h_{\text{Disch}} \leq \lambda_{\text{DR}} \cdot BESS^h_{\text{D}} \tag{23}$$

Since energy (E) and power (P) are related by $E = P \cdot \Delta t$, and the time interval Δt is 1 hour, energy E^h (in Wh) and power P^h (in W) are numerically equivalent in each hour time step, though they represent different physical quantities. The BESS cannot charge and discharge simultaneously:

$$I^h_{\text{Ch}} + I^h_{\text{Disch}} \leq 1 \tag{24}$$

where I^h_{Ch} and I^h_{Disch} are 1 if the battery is charged or discharged, respectively.

SOC(h) is the stored energy in $BESS$ at time h. It must stay within predefined limits (SOC_{min} and SOC_{max}) for safe operation. When energy is injected or taken from the battery, we consider the charging and discharging efficiencies (η_{Ch} and η_{Disch}), respectively. The described conditions are formulated as follows:

$$SOC_{\text{h}} = SOC_{\text{h-1}} + \eta_{\text{Ch}} \cdot P^h_{\text{Ch}} \cdot \Delta t - \frac{P^h_{\text{Disch}} \cdot \Delta t}{\eta_{\text{Disch}}} \tag{25}$$

$$SOC_{\text{min}} \leq SOC_{\text{h}} \leq SOC_{\text{max}} \tag{26}$$

The $DoD(h)$ measures battery usage and is calculated as the amount of energy drawn from the storage, expressed as a percentage of nominal installed battery capacity (E^{max}_{BESS}):

$$DoD(h) = 1 - \frac{SOC(\text{h})}{E^{max}_{\text{BESS}}} \tag{27}$$

In addition, the $DoD(h)$ is non-negative and must stay below the maximum allowable limit (DoD_{max}), such that $0 \leq DoD(h) \leq DoD_{\text{max}}$, where DoD_{max} is predefined in each simulation to meet the requirement of reserving a specified portion of the battery capacity. This reserved capacity ensures that the system can handle potential power outages according to their probability and severity as explained in [8].

The power balance constraint for the problem is given by:

$$P^h_{\text{grid}} + P^h_{\text{PV}} + P^h_{\text{Discharge}} = P^h_{\text{Load}} + P^h_{\text{W}} + P^h_{\text{Charge}} \tag{28}$$

This ensures that the total power supply equals the total power demand at any time h.

IV. Numerical results and discussion

This paper analyses a hybrid power system for a BS in Turin, Italy. The analysis relies on actual hourly energy consumption data measured from a multi-frequency BS over one month, which provides a realistic and complete load profile. PV generation is modeled using data from NASA's POWER meteorological database. The photovoltaic technology employed in this study is the Canadian Solar MaxPower CS6U-340M module.

TABLE II: Comparison of System Metrics (Costs Aggregated Over 20-Year System Lifetime.)

Max DoD (%)	PV Panel (kW)		Li-ion Battery (kWh)		NPC ($)		LCOE ($/kWh)		E_{W}^{h} (kWh)	
	With Aging	*Without Aging*	*With Aging*	*Without Aging*	*With Aging*	*Without Aging*	*With Aging*	*Without Aging*	*With Aging*	*Without Aging*
80	3.66	4.17	3	10	41767	39801	0.35	0.32	5936	1371
70	3.37	4.17	3	11	41908	40294	0.34	0.32	6651	1353
60	3.95	4.17	10	12	41618	40964	0.33	0.33	6264	1414
50	3.65	3.99	7	7	41736	41774	0.34	0.34	6401	1338
40	3.37	4.17	4	3	41962	42177	0.34	0.33	6556	1746
30	3.37	4.17	3	3	42064	42424	0.34	0.32	6548	1936
20	3.36	3.40	3	3	42426	42677	0.35	0.35	6442	1300
10	3.40	3.38	3	3	42453	42720	0.35	0.35	6523	1327

The energy storage system employed is a lithium-ion system, whose aging and performance data are adopted from [12]. We formulate the electricity cost model based on [13]. To test the efficacy of the suggested optimization framework and the battery degradation model, we consider the following two scenarios:

1) **Case I: Basic System Configuration (Ideal Battery—IB)** The system planning does not take into account battery aging.
2) **Case II: System Planning with Battery Aging (Real Battery—RB)** The present case integrates the suggested segment-based battery aging model, which emulates the realistic aging pattern of a lithium-ion battery over a specified period.

To further assess the performance of our segment-based aging model, we compare its outcomes with those from a conventional Rainflow-based degradation estimation technique, as described in [11].

Key Performance Indicators (KPIs)

This study employs various Key Performance Indicators (KPIs) to assess the performance of the hybrid energy system: (1) **Net Present Cost (NPC)**: The aggregate expense of system installation and operation throughout its lifespan, adjusted to present value through discounting. It includes CAPEX and OPEX. (2) **Levelized Cost of Energy (LCOE)**: The mean expenditure per energy unit generated throughout the system's lifespan. The calculation is performed by dividing total costs by total energy generated. (3) **Curtailed PV Production** (E_{W}^{h}): The quantity of PV energy produced but not employed.

Comparative Analysis of Case I and Case II

This section compares system sizing strategies in IB, and RB scenarios. Table II summarizes the results, comparing system KPIs with and without aging consideration across various maximum DoD levels. When aging is considered, PV panel sizes and battery capacities are generally smaller, while NPC increases slightly due to higher long-term costs. LCOE remains relatively stable but E_{W}^{h} is higher due to the consideration of battery aging. Aging costs influence charge and discharge decisions, reducing the battery's ability to store excess energy during peak PV production, which increases energy waste. These results underscore the impact of DoD and aging on system sizing, costs, and energy utilisation.

Based on Table II, in IB, the optimal solution occurs at a maximum DoD of 80%, with a battery size of 10 kWh and a PV panel size of 4.17 kW. In contrast, in the RB scenario at the same DoD level, the battery size is significantly reduced to 3 kWh, and the PV panel size is reduced to 3.66 kW. This difference demonstrates that without considering aging, the system allows for deeper discharges and larger component sizing to maximise energy utilisation, leading to lower NPC values in Case I at this DoD level ($39,801 vs $41,767).

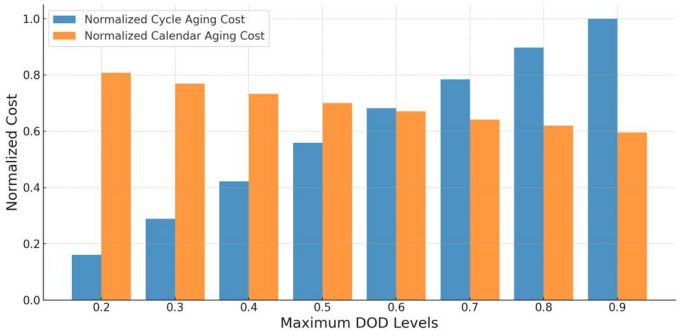

Fig. 3: Normalized Cycle and Calendar Aging Costs for Different Maximum DoD Levels.

In RB scenario, the optimal solution shifts to a DoD of 60%, where the battery size is 10 kWh, and the PV panel size is 3.95 kW. When compared to IB at the same DoD level, where the battery size is also 12 kWh and the PV panel size is larger at 4.17 kW, the system sizing in RB is more conservative due to the aging considerations.

Based on the optimal battery size of 10 kWh from the RB scenario, we conduct a sensitivity analysis on the effects of different maximum allowable DoD levels on system performance and aging. This part examines how varying the DoD impacts the trade-off between calendar and cycle aging. Fig. 3 shows the normalised cycle and calendar aging costs. The blue bars represent cycle aging costs, which increase with DoD, while the orange bars represent calendar aging costs, which decrease. Higher DoD increases usable capacity, accelerates cycle aging, and reduces calendar aging, while lower DoD decreases cycle aging but increases calendar aging due to high SOC. The intersection at DoD = 0.6 confirms the optimal trade-off between battery aging contributions.This is consistent with Table II, which also shows optimal performance at DoD = 0.6 under aging-aware planning.

Segment-Based Aging versus Rainflow Estimation

To evaluate the *practical accuracy and computational tractability* of the proposed segment-based cycle aging model,

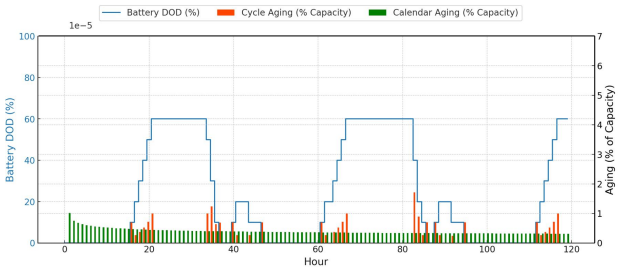

(a) Segment-based model

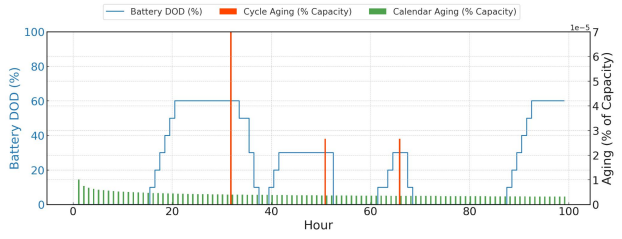

(b) Rainflow-based approach

Fig. 4: Comparison of battery degradation methods

we compare its performance against the conventional Rainflow-based approach from [5] under the RB scenario with an optimal battery size of 10 kWh.

Fig. 4 illustrates the fundamental differences between the two methods. The *segment-based model* (Fig. 4a) updates aging at each time step by directly tracking DoD transitions, thereby capturing partial and incomplete cycles that frequently occur under variable PV generation and dynamic BS loads. The blue stepped line shows the battery DoD profile, while the orange and green bars indicate incremental cycle and calendar aging, respectively. Spikes in cycle aging correspond to periods of deeper discharge, whereas the steady progression of calendar aging reflects SOC-dependent degradation over time.

In contrast, the *Rainflow-based approach* (Fig. 4b) estimates cycle aging only upon the detection of complete charge-discharge cycles, resulting in *delayed and less frequent aging updates*. This limitation can lead to the underestimation of degradation under partial cycling conditions, which is significant in hybrid PV-battery systems where full cycles are often incomplete due to intermittent PV production and varying load demands.

From a computational standpoint, the segment-based model seamlessly integrates within MILP-based planning frameworks, adding negligible computational overhead while enabling real-time, aging-aware optimization. In contrast, Rainflow analysis typically requires offline post-processing, limiting its applicability in real-time control strategies. Table III quantifies the differences between methods for the operational cost over one month, showing that the proposed segment-based model reduces cycle aging by **65%** compared to the no-aging baseline and achieves an additional **10% reduction** relative to the Rainflow method, while maintaining competitive operational costs. Calendar aging remains similar across methods due to consistent SOC and temperature conditions during operation.

TABLE III: Comparison of Battery Aging and Operating

Method	**Cal. Aging (%)**	**Cyc. Aging (%)**	**Cost (€)**
IB (No Aging)	0.193	0.391	70
RB (Rainflow)	0.196	0.150	79
RB (Segment)	0.194	0.135	82

V. Conclusion and Future Work

This paper proposes a novel segment-based battery aging model for the planning and operation of 5G BS MILP-based PV batteries. By tracking real-time DoD transitions through full, partial, and incomplete cycles, the model allows cycle and calendar aging to be accurately estimated without resorting to offline techniques such as Rainflow.

Compared to conventional approaches, it achieves up to 10% cycle aging reduction and improves energy planning decisions at every time slot. The proposed framework also minimises operational expenditure and maximises battery lifespan, which is validated with real urban traffic and solar data. As future work, we plan to generalise the framework to multi-node cooperative systems and include stochastic PV forecasting.

References

[1] Keysight Technologies, "Next Generation Wireless: A Guide to the Fundamentals of 6G," [Online]. Available: https://www.keysight.com/at/de/assets/7123-1050/ebooks/Next-Generation-Wireless-A-Guide-to-the-Fundamentals-of-6G.pdf [Accessed: Jan. 22, 2025].

[2] A. Israr *et al.*, "Renewable energy powered sustainable 5G network infrastructure: Opportunities, challenges and perspectives," *Journal of Network and Computer Applications*, vol. 175, p. 102910, 2021.

[3] A. I. Osman *et al.*, "Cost, environmental impact, and resilience of renewable energy under a changing climate: A review," *Environmental Chemistry Letters*, vol. 21, no. 2, pp. 741–764, 2023.

[4] G. Vallero *et al.*, "Network resilience and sustainability: Renewable energy-based solutions," *IEEE Communications Magazine*, vol. 63, no. 5, pp. 118–124, May 2025, doi: 10.1109/MCOM.001.2300685.

[5] T. Gewald, *et al.*, "Accelerated aging characterization of lithium-ion cells: Using sensitivity analysis to identify the stress factors relevant to cyclic aging," *Batteries*, vol. 6, no. 1, p. 6, 2020.

[6] M. Amini, *et al.* "Optimal Scheduling and Cost-Benefit Analysis of Lithium-Ion Batteries Based on Battery State of Health," *IEEE Access*, vol. 11, pp. 1359-1371, 2023, doi: 10.1109/ACCESS.2022.3232282.

[7] G. Yüksek, *et al.*, "Effect of the depth of discharge and C-rate on battery degradation and cycle life," in *2023 14th International Conference on Electrical and Electronics Engineering (ELECO)*, 2023, IEEE.

[8] M. R. Jokar, *et al.*, "Stationary and mobile storages-based renewable off-grid system planning considering storage degradation cost based on information-gap decision theory optimization," *Journal of Energy Storage*, vol. 58, p. 106389, 2023.

[9] N. Q. Minh, *et al.*, "A mixed-integer linear programming model for microgrid optimal scheduling considering BESS degradation and RES uncertainty," *Journal of Energy Storage*, vol. 104, p. 114663, 2024.

[10] R. Lehr, *et al.*, "Depreciation and Early Plant Retirements," *Energy Innovation: Policy & Technology LLC*, Dec. 2018. [Online]. Available: https://www.energyinnovation.org/

[11] M. Amini, *et al.*, "Optimal energy management of battery with high wind energy penetration: A comprehensive linear battery degradation cost model," *Sustainable Cities and Society*, vol. 93, p. 104492, 2023.

[12] M. A. Ashraf, *et al.*, "Designing an optimized configuration for a hybrid PV/Diesel/Battery Energy System based on metaheuristics: A case study on Gobi Desert," *Journal of Cleaner Production*, vol. 270, pp. 122467, 2020, doi: 10.1016/j.jclepro.2020.122467.

[13] J. Reneses, *et al.*, "Distribution Pricing: Theoretical Principles and Practical Approaches," *IET Generation, Transmission & Distribution*, vol. 8, no. 10, pp. 1645–1655, 2014.